Supplementary Materials

Synergistic dipole and pseudo-hydrogen bonding in phosphate electrolytes for stable elevated temperature lithium batteries

Chengcheng Tao[1], Zhiqiang Han[4], Yin Shen[1], Yike He[1], Yuting Wang[1], Gen Li[1], Bo Zhao[1], Mingshan Wang[1,2,3,*], Michael Zaiser[1,5,*], Xing Li[1,2,3,*]

[1]School of New Energy and Materials, Southwest Petroleum University, Chengdu 610500, Sichuan, China.
[2]SILK ROAD Research Center of Sustainable Energy Conversion and Utilization, Southwest Petroleum University, Chengdu 610500, Sichuan, China.
[3]Vanadium Flow Battery Engineering Research Center of Sichuan Province, Southwest Petroleum University, Chengdu 610500, Sichuan, China.
[4]Beijing Advanced Innovation Center for Materials Genome Engineering, Center for Green Innovation, School of Mathematics and Physics, University of Science and Technology Beijing, Beijing 100083, China.
[5]Department Werkstoffwissenschaften, Lehrstuhl für Werkstoffsimulation (WW8), FAU Erlangen-Nürnberg, Dr. Mack Strasse 77, Fürth 70962, Germany.

Correspondence to: Dr. Mingshan Wang, Dr. Xing Li, School of New Energy and Materials, Southwest Petroleum University, Chengdu 610500, Sichuan, China; SILK ROAD Research Center of Sustainable Energy Conversion and Utilization, Southwest Petroleum University, Chengdu 610500, Sichuan, China; Vanadium Flow Battery Engineering Research Center of Sichuan Province, Southwest Petroleum University, Chengdu 610500, Sichuan, China. E-mail: wangmingshan@swpu.edu.cn; lixing@swpu.edu.cn; Dr. Michael Zaiser, School of New Energy and Materials, Southwest Petroleum University, Chengdu 610500, Sichuan, China; Department Werkstoffwissenschaften, Lehrstuhl für Werkstoffsimulation (WW8), FAU Erlangen-Nürnberg, Dr. Mack Strasse 77, Fürth 70962, Germany. E-mail: michael.zaiser@fau.de

NOTE: All figures in the Supplementary Materials were plotted using Origin 2018 and assembled with Microsoft PowerPoint (PPT).

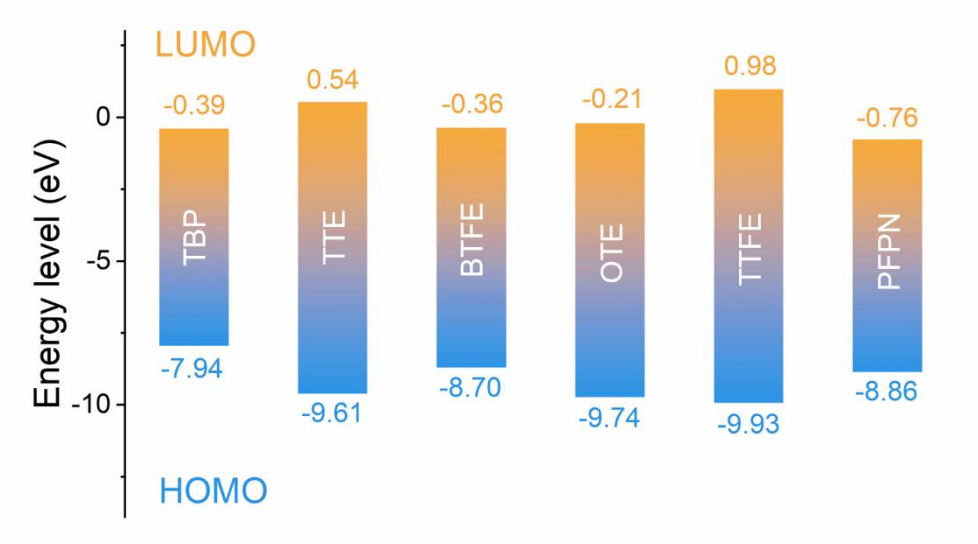

Supplementary Figure 1 The calculated HOMO and LUMO energy level (eV) of previously reported fluorinated diluents

Note: HOMO/LUMO energy level was calculated using DFT at the B3LYP/6-31G** level

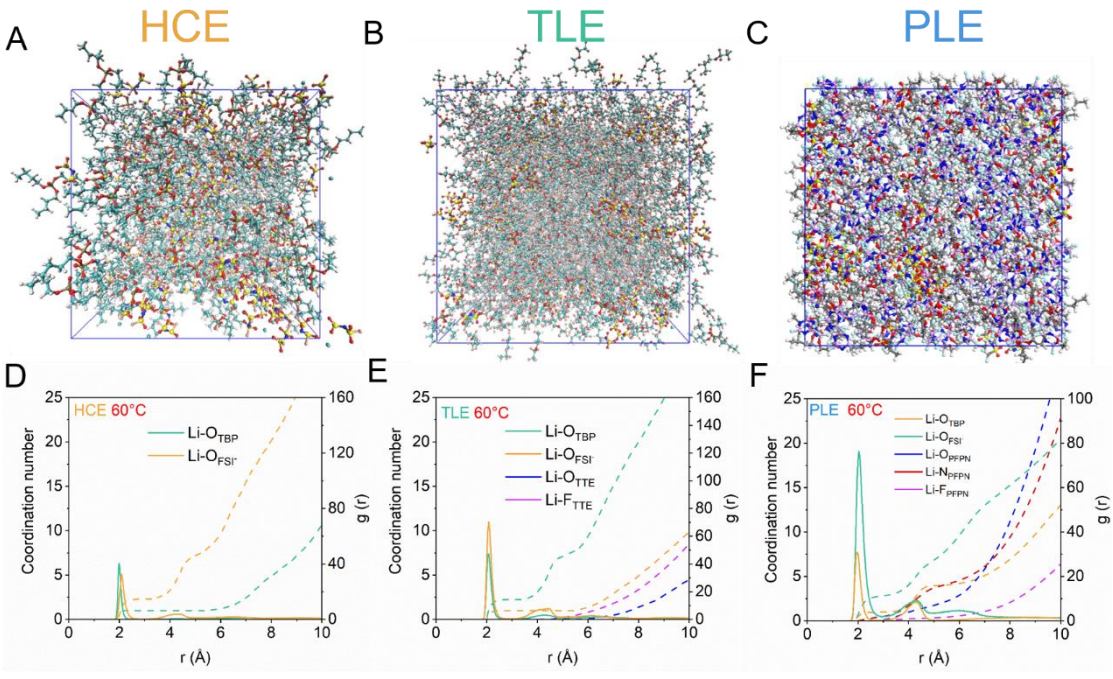

Supplementary Figure 2 At 60°C, MD simulation snapshots of **(A)** HCE, **(B)** TLE and **(C)** PLE. Radial distributions (RDF) and corresponding coordination of Li-O_{TBP}, Li-O_{FSI}⁻, Li-O_{PFPN}, Li-N_{PFPN}, and Li-F_{PFPN} pairs calculated from MD simulation of **(D)** HCE, **(E)** TLE and **(F)** PLE.

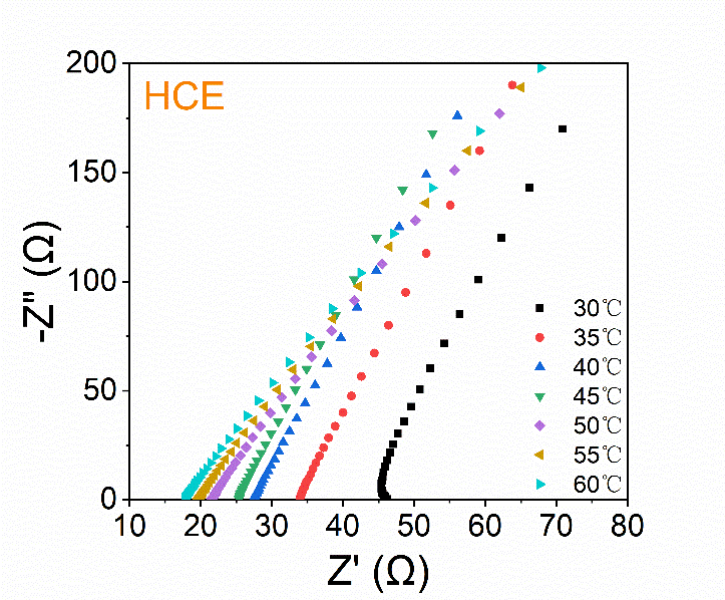

Supplementary Figure 3 The impedance value of the stainless-steel symmetrical battery (SS||SS) assembled using HCE electrolyte at temperatures ranging from 30 to 60°C.

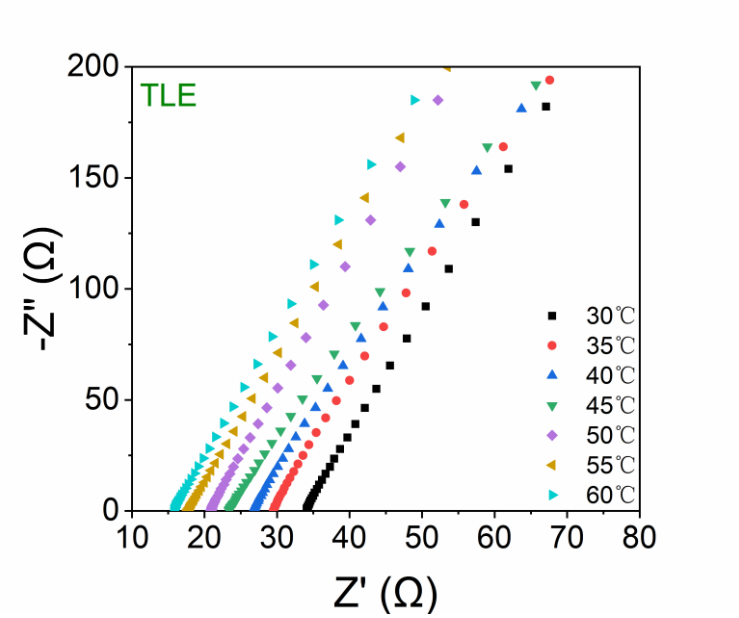

Supplementary Figure 4 The impedance value of the stainless-steel symmetrical battery (SS||SS) assembled using TLE electrolyte at temperatures ranging from 30 to 60°C.

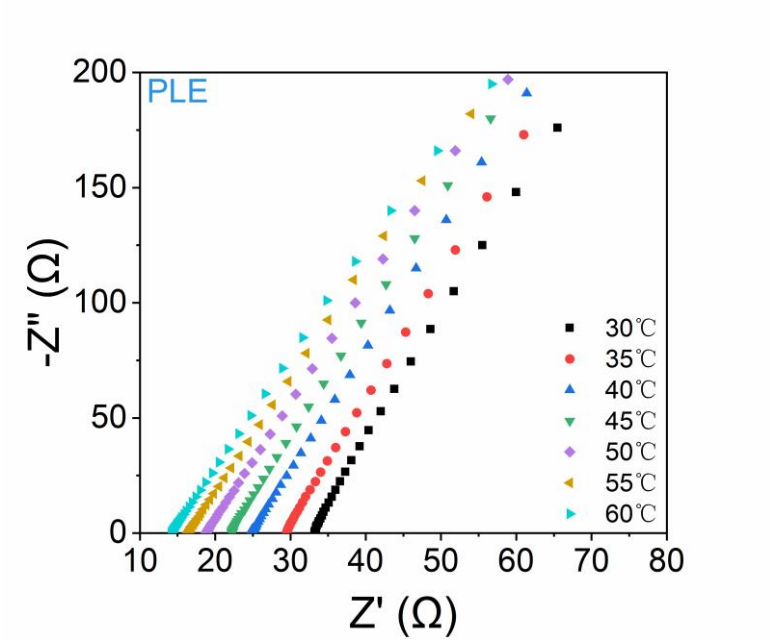

Supplementary Figure 5 The impedance value of the stainless-steel symmetrical battery (SS||SS) assembled using PLE electrolyte at temperatures ranging from 30 to 60°C.

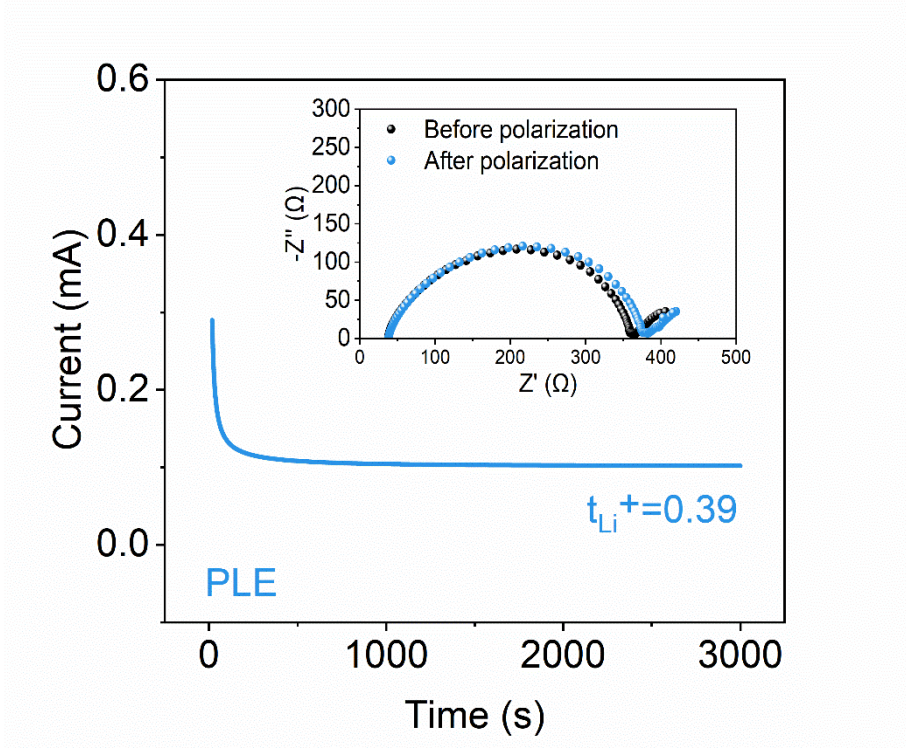

Supplementary Figure 6 Chronoamperometry (CA) of Li||Li cell with PLE electrolyte and the corresponding EIS spectra (the inset) before and after polarization.

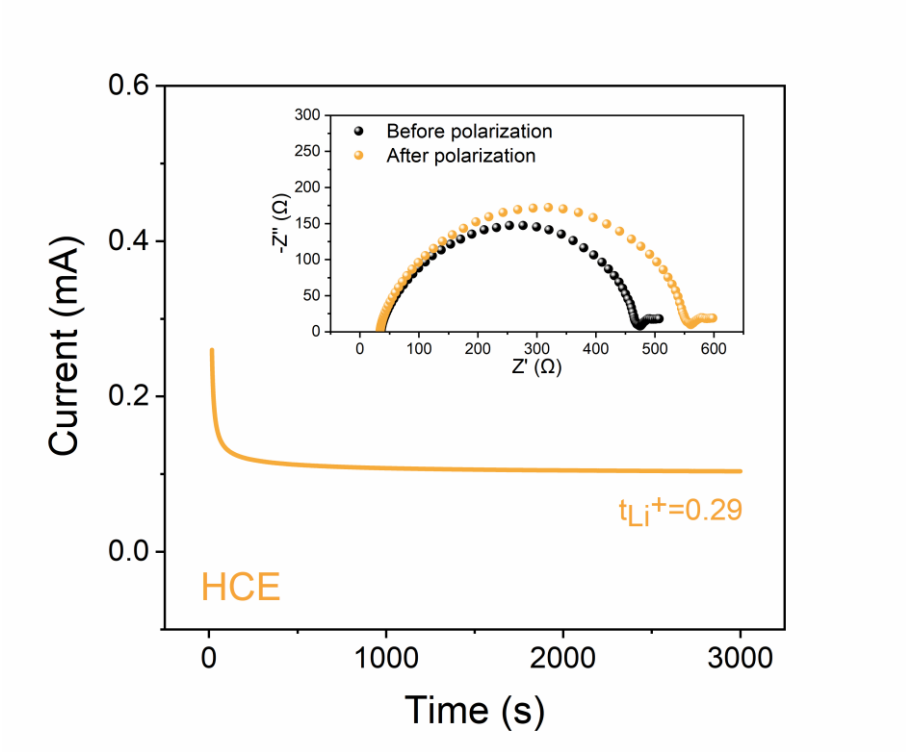

Supplementary Figure 7 Chronoamperometry (CA) of Li||Li cell with HCE electrolyte and the corresponding EIS spectra (the inset) before and after polarization.

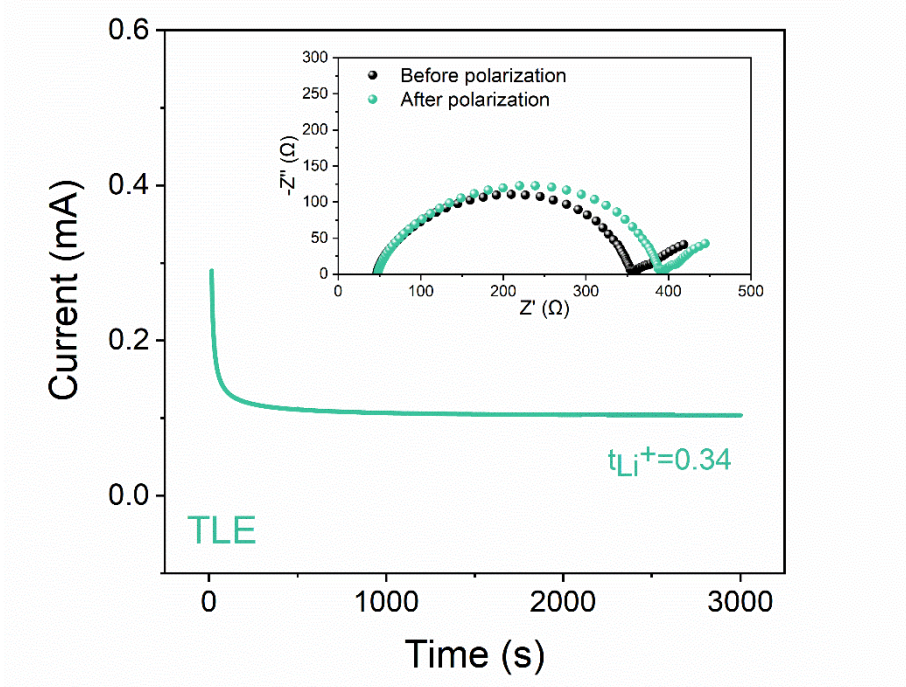

Supplementary Figure 8 Chronoamperometry (CA) of Li||Li cell with TLE electrolyte and the corresponding EIS spectra (the inset) before and after polarization.

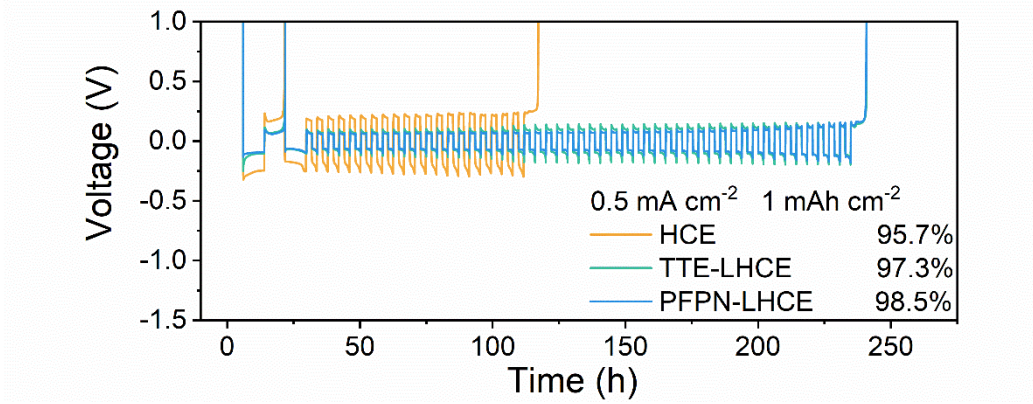

Supplementary Figure 9 Coulombic efficiency of Li||Cu cells in HCE, TLE and PLE electrolytes tested by Modified Aurbach's measurement.

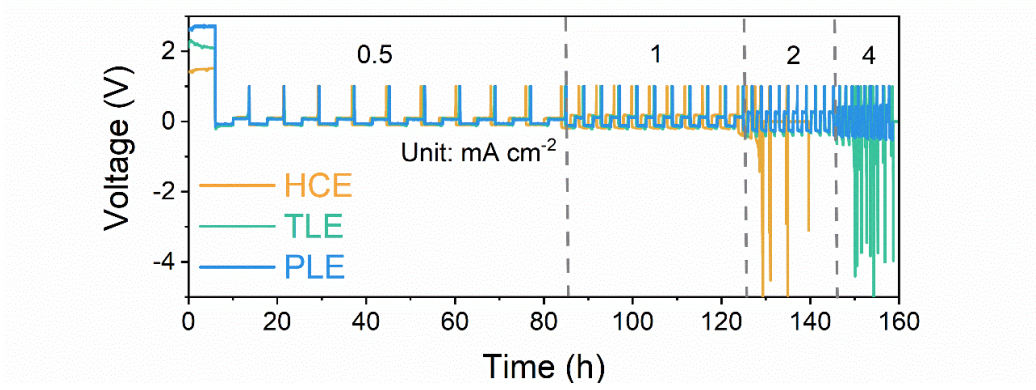

Supplementary Figure 10 Charging and discharging voltage profiles of Li||Cu cells in HCE, TLE and PLE electrolytes at current densities of 0.5, 1, 2, and 4 mA·cm^{-2} with a specific capacity of 1 mAh·cm^{-2}.

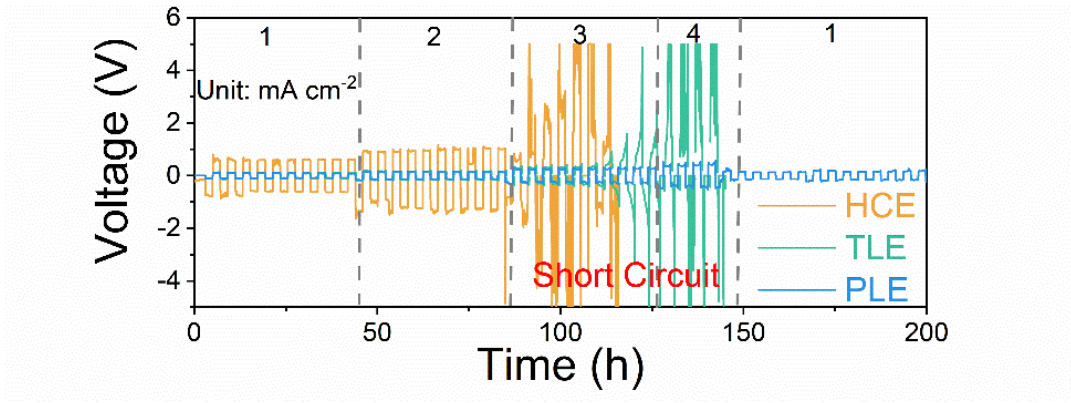

Supplementary Figure 11 Voltage-time profiles of Li||Li cells in HCE, TLE and PLE electrolytes at current densities of 1, 2, 3, and 4 mA·cm^{-2} with a specific capacity of 1 mAh·cm^{-2}.

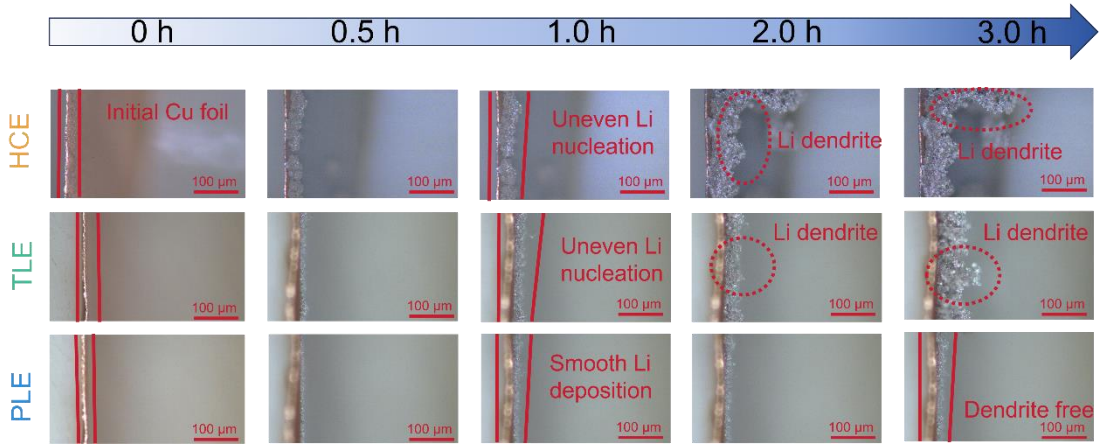

Supplementary Figure 12 In-situ optical images of the Li deposition morphology at the Li metal anode in HCE, TLE and PLE electrolytes.

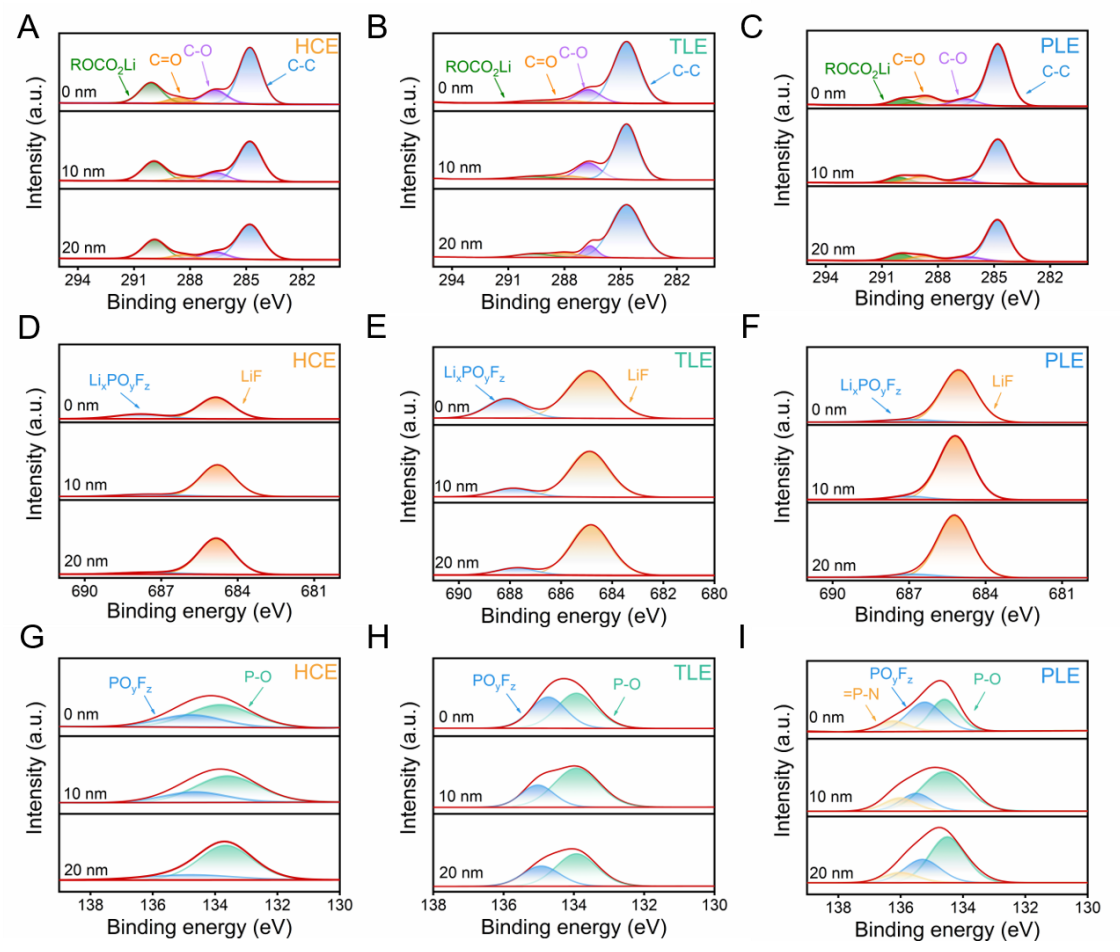

Supplementary Figure 13 XPS analysis of C 1s, F 1s, and P 2p of Li metal anodes after 50 cycles in HCE, TLE and PLE electrolytes at various sputtering depths (0, 10, 20 nm)

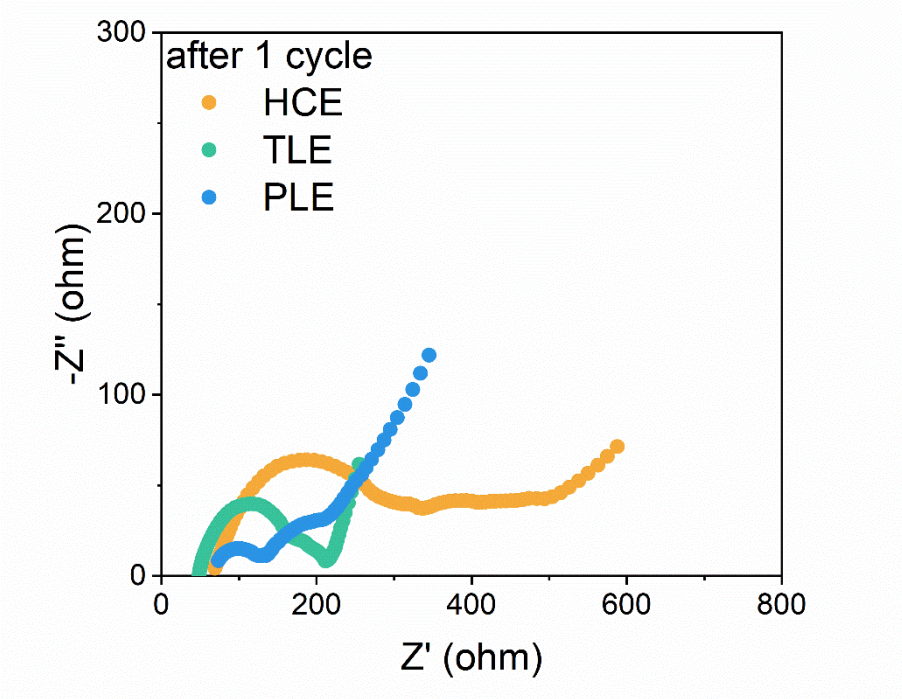

Supplementary Figure 14 Alternating current (AC) impedance spectra after 1 cycle at 0.5C charge\discharge in HCE, TLE and PLE electrolytes

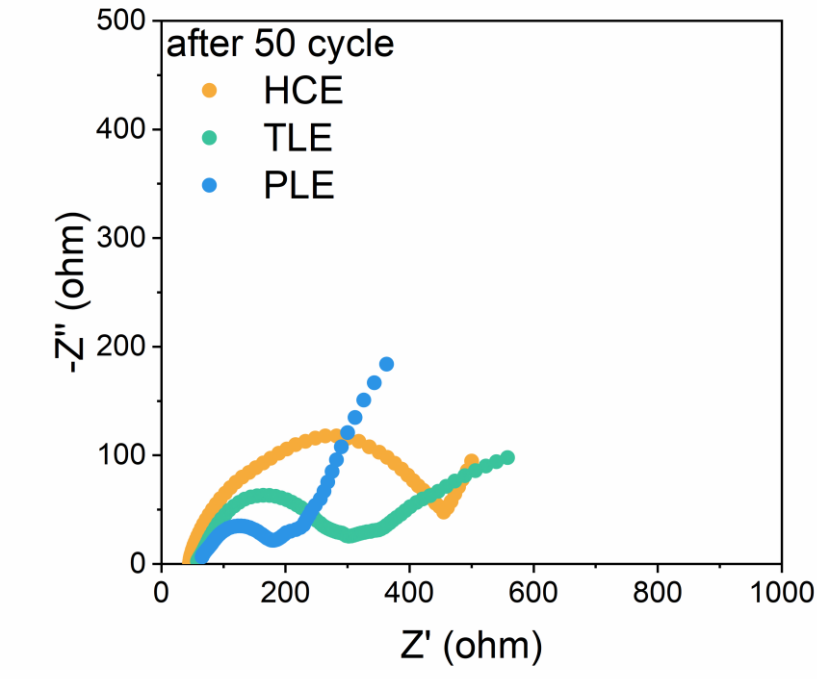

Supplementary Figure 15 Alternating current (AC) impedance spectra after 50 cycles at 0.5C charge\discharge in HCE, TLE and PLE electrolytes

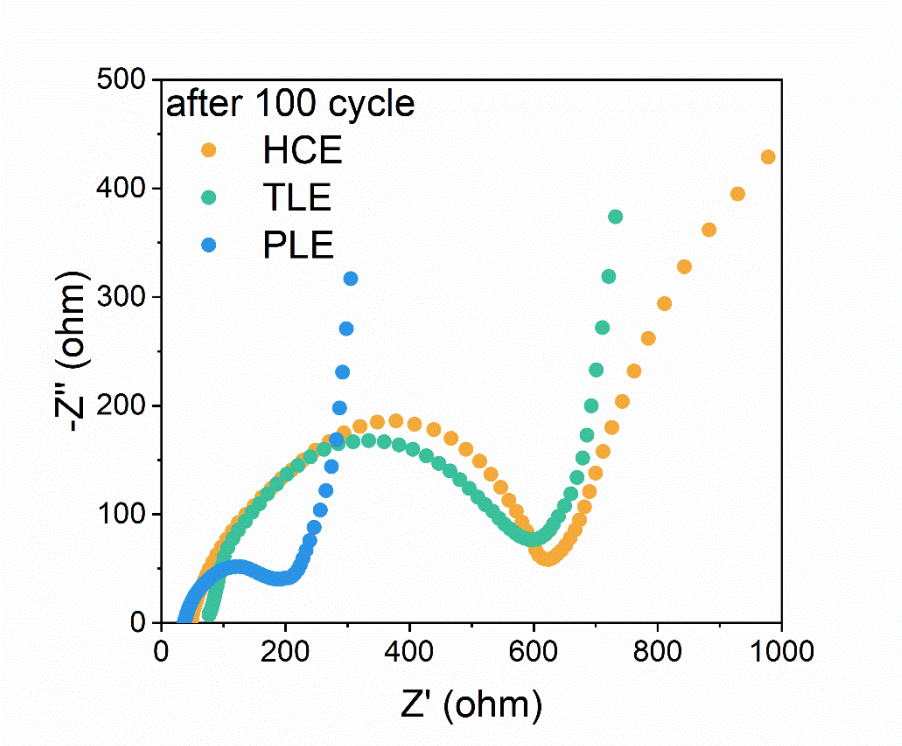

Supplementary Figure 16 Alternating current (AC) impedance spectra after 100 cycles at 0.5C charge\discharge in HCE, TLE and PLE electrolytes

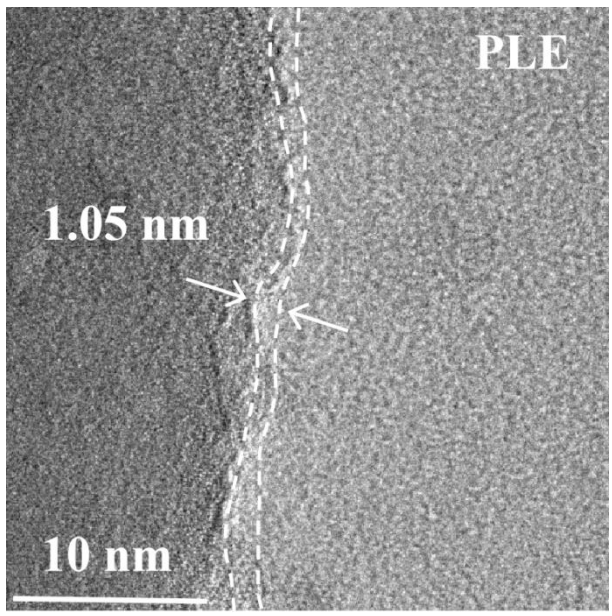

Supplementary Figure 17 TEM images of NCM811 at 60°C after 50 cycles in PLE.

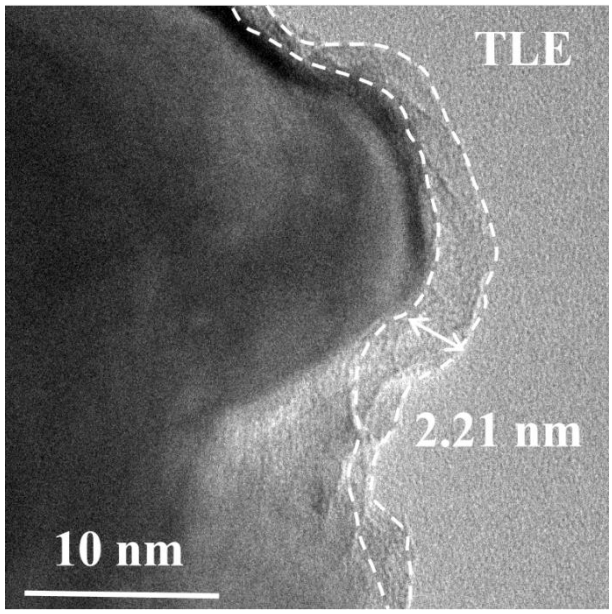

Supplementary Figure 18 TEM images of NCM811 at 60°C after 50 cycles in TLE.

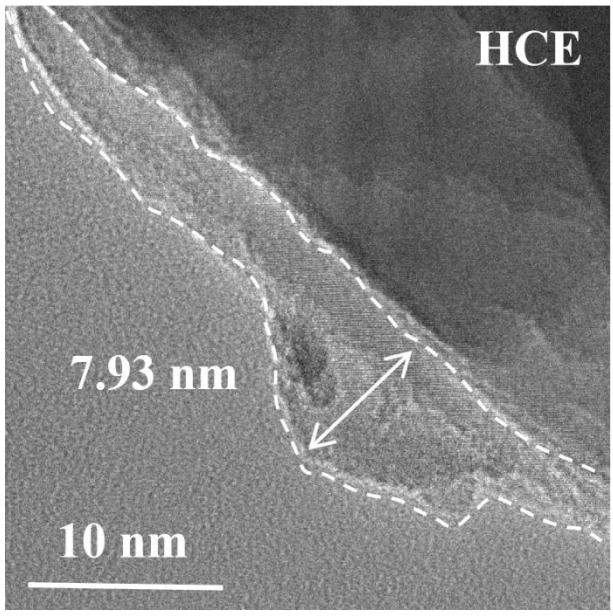

Supplementary Figure 19 TEM images of NCM811 at 60°C after 50 cycles in HCE.

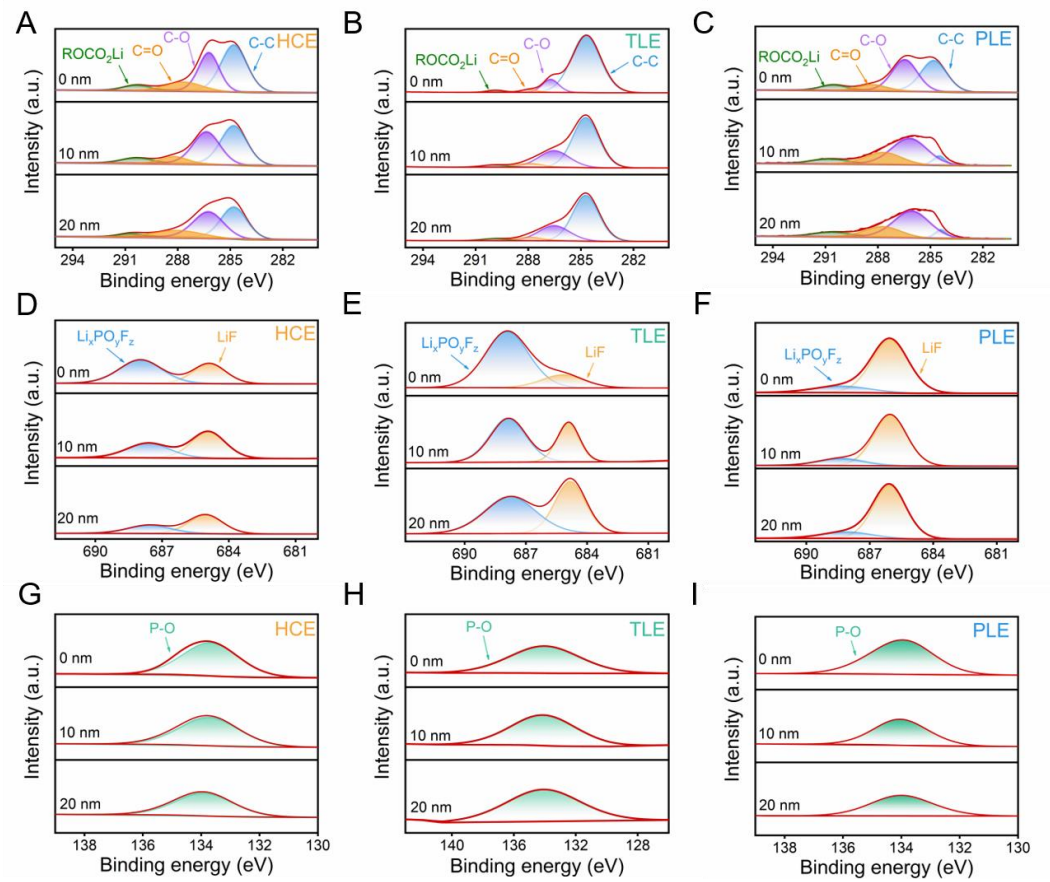

Supplementary Figure 20 XPS analysis of C 1s, F 1s, and P 2p of NCM811 after 50 cycles in (A, D, G) HCE, (B, E, H) TLE and (C, F, I) PLE electrolytes at various sputtering depths (0, 10, 20 nm)

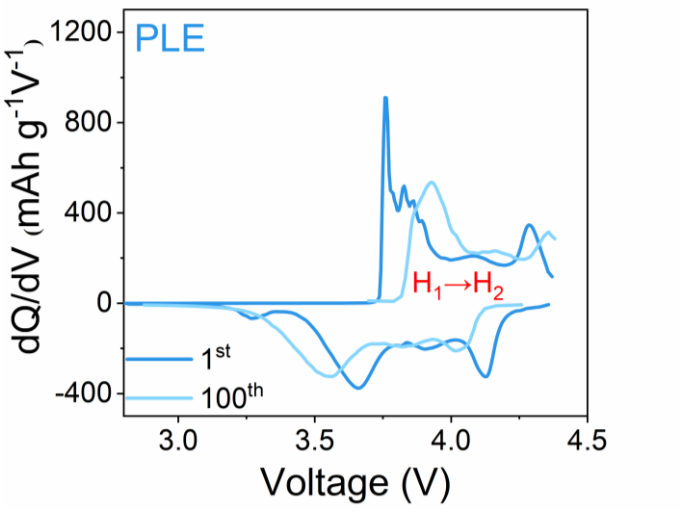

Supplementary Figure 21 The dQ/dV curves from 1st to 100th charging and discharging process in PLE electrolyte.

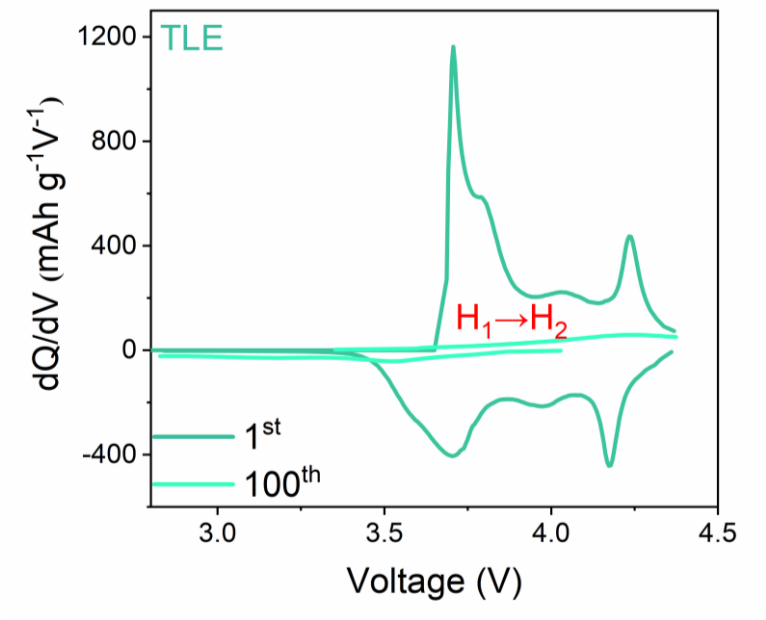

Supplementary Figure 22 The dQ/dV curves from 1st to 100th charging and discharging process in TLE electrolyte.

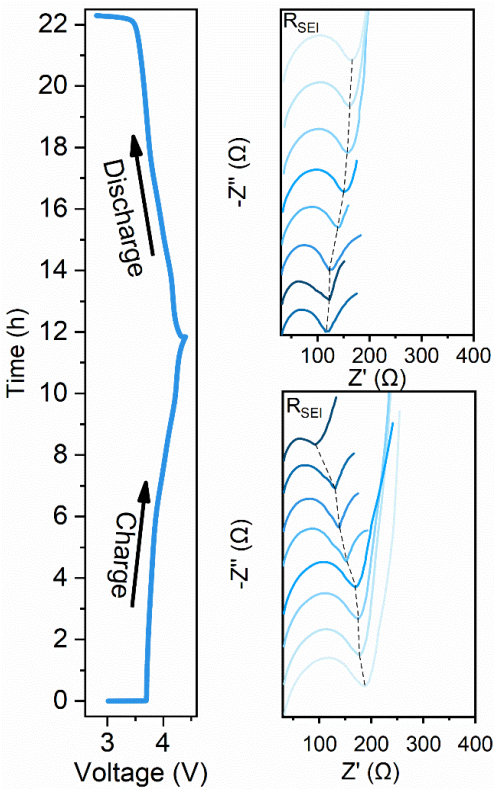

Supplementary Figure 23 The initial charge/discharge curve of Li||NCM811 cells measured at 0.1C and the corresponding impedance spectra collected during initial charge/discharge are displayed in PLE

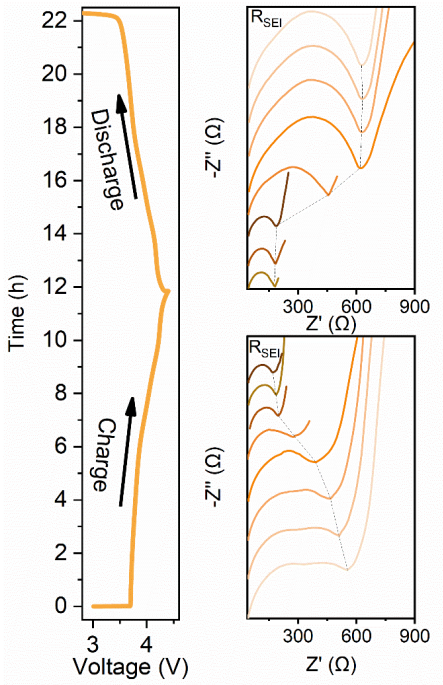

Supplementary Figure 24 The initial charge/discharge curve of Li||NCM811 cells measured at 0.1C and the corresponding impedance spectra collected during initial charge/discharge are displayed in HCE

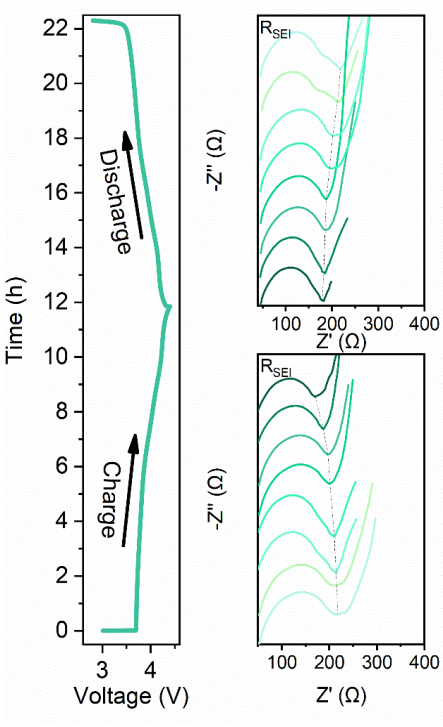

Supplementary Figure 25 The initial charge/discharge curve of Li||NCM811 cells measured at 0.1C and the corresponding impedance spectra collected during initial charge/discharge are displayed in TLE

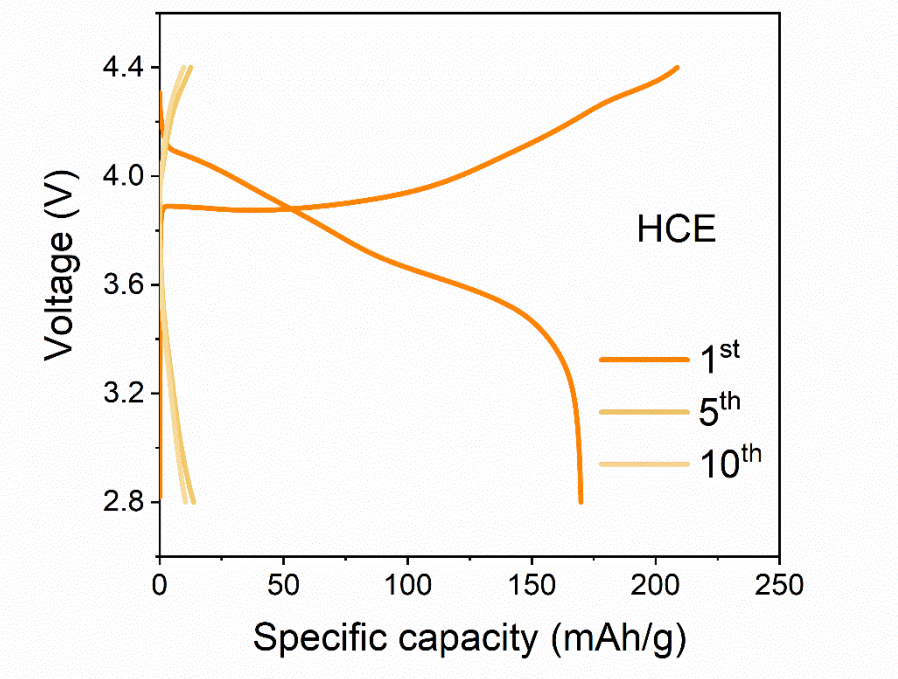

Supplementary Figure 26 Charge/discharge curves of the Li (50 μm) || NCM811 (9.2 mg cm^{-2}) cells at 30°C in HCE electrolyte.

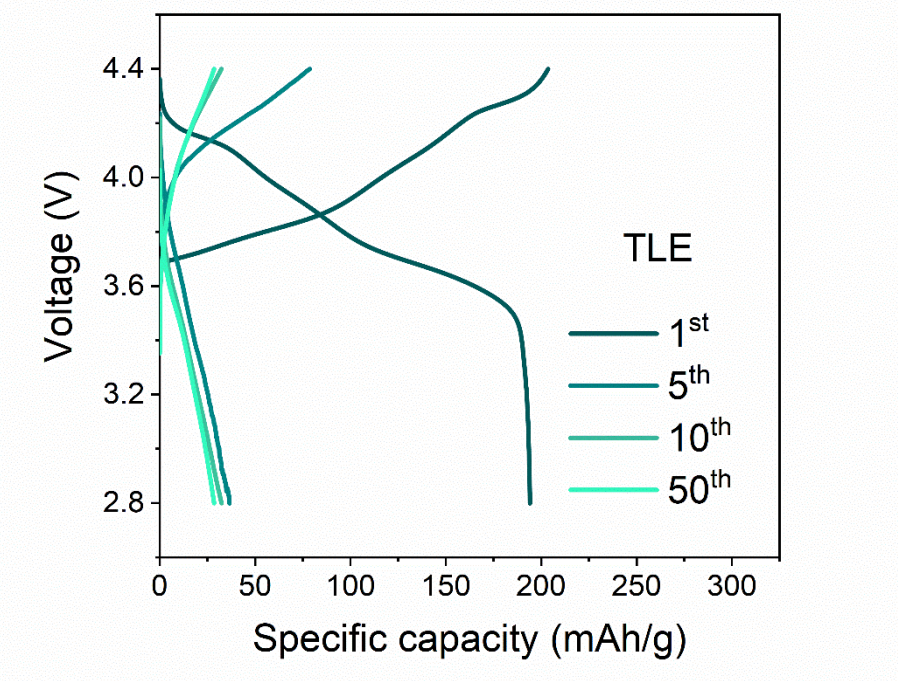

Supplementary Figure 27 Charge/discharge curves of the Li (50 μm) || NCM811 (9.2 mg cm^{-2}) cells at 30°C in TLE electrolyte.

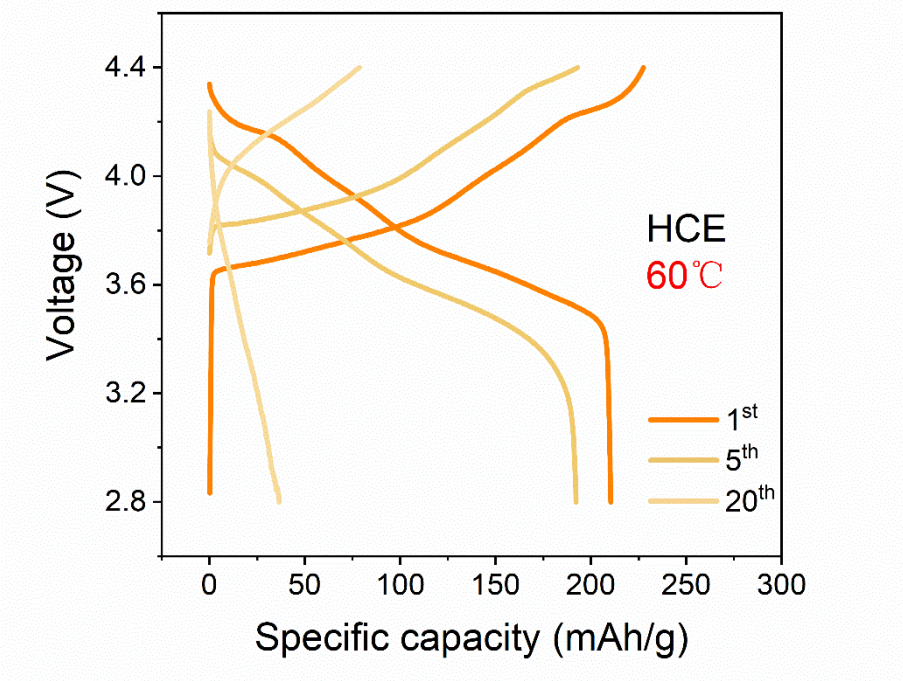

Supplementary Figure 28 Charge/discharge curves of the Li (50 μm) || NCM811 (9.2 mg cm^{-2}) cells at 60°C in HCE electrolyte.

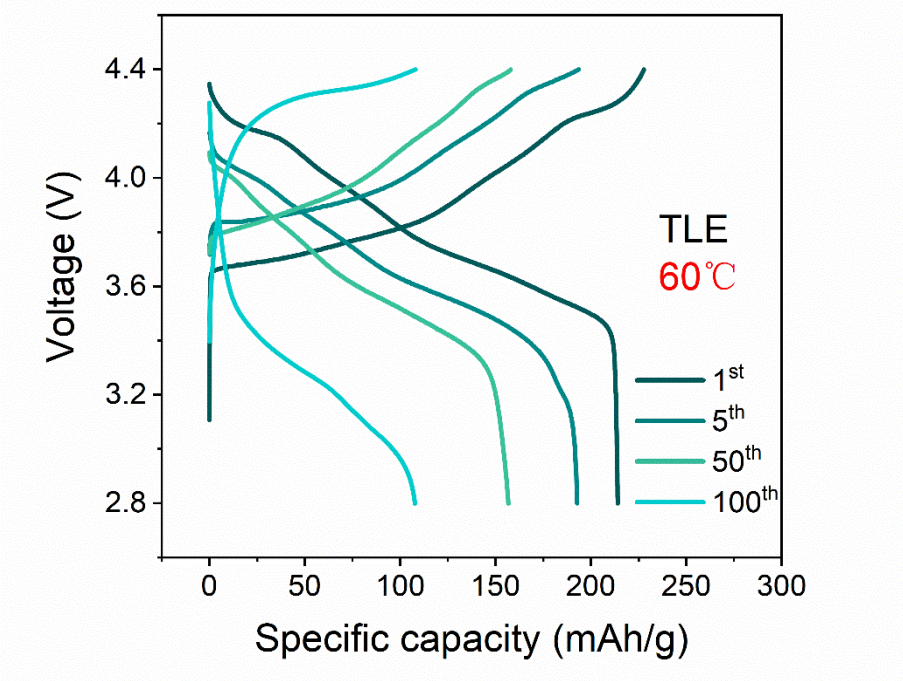

Supplementary Figure 29 Charge/discharge curves of the Li (50 μm) || NCM811 (9.2 mg cm^{-2}) cells at 60°C in TLE electrolyte.

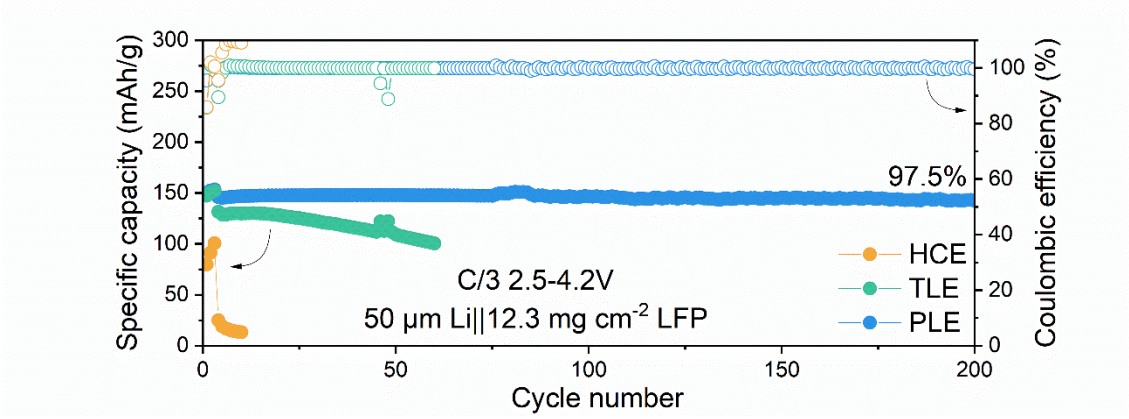

Supplementary Figure 30 Cycling performance of the Li (50μm) || LFP (12.3mg cm^{-2}) cells with HCE, TLE and PLE electrolytes at 30°C.

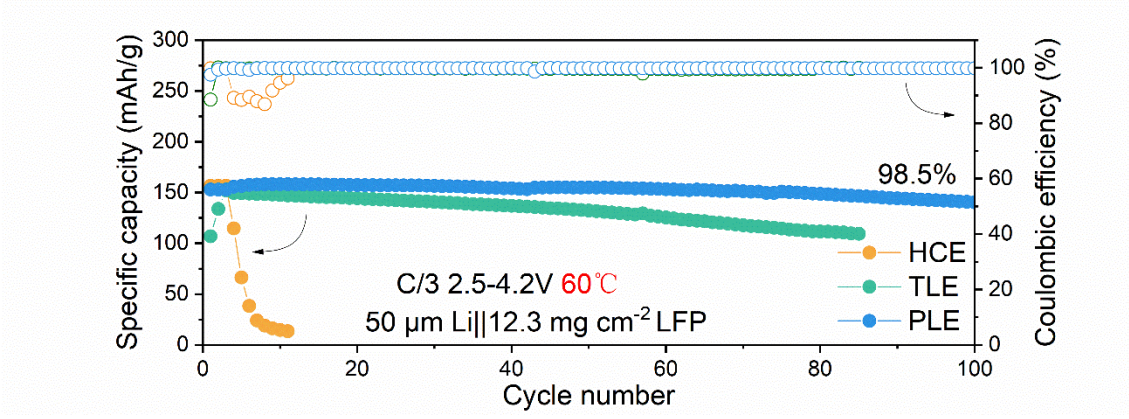

Supplementary Figure 31 Cycling performance of the Li (50μm) || LFP (12.3mg cm^{-2}) cells with HCE, TLE and PLE electrolytes at 60°C.

Supplementary Table 1. AC impedance values of Li||NCM811 cells with HCE, TLE and PLE electrolytes.

Cycle	Electrolyte	R_e (Ω)	R_{SEI} (Ω)	Rct(Ω)
	HCE	85.5	237.6	197.2
1	TLE	76.6	149.8	111.6
	PLE	65.3	53.2	98.3
	HCE	69.2	471.6	381.9
50	TLE	57.7	305.4	88.5
	PLE	65.4	104.1	62.1
	HCE	48.7	603.7	415.0
100	TLE	48.4	598.3	309.8
	PLE	73.2	186.8	184.8

Supplementary Table 2. The electrochemical performance of Li||NCM811 in cycle stability, compared with published literature.

Electrolytes	Cell parameters		Electrochemical performance	Ref
	Anode||Cathode	Cathode loading (mg cm^{-2})	Cycle stability	
LiFSI:TBP:PFPN (1:1.2:5 by mol.)	Li(50 μm)||NCM811	21.2	C/2 90.3% (100 cycles)	This work
3M LiFSI TBP: DME (7:3 by vol.)	Li(50 μm)||NCM811	15.4	C/2: 88% (120 cycles)	[1]
3M LiFSI TBP: G2 0.2MLiDFOB (7:3 by vol.)	Li(50 μm)||NCM811	8.3	C/2: 86.2% (200 cycles)	[2]
LiFSI:TEP:PFPN (0.75:1:1 by mol.)	Li(50 μm)||NCM811	9	C/3 96.8% (100 cycles)	[3]
LiTFSI: TFEP (1:2 by mol.)	Li(50 μm)||NCM811	7.5	C/10 82.7% (100 cycles)	[4]
LiFSI: TFEP: PFPN (1:1.7:4 by mol.)	Li(50 μm)||NCM811	8.2	C/3: 82.3% (100 cycles)	[5]

Supplementary Table 3. Pouch cell parameters of the Li||NCM811 full cells.

NCM811 Cathode	**Pouch cell Parameters**	
	Active material Loading	94.5%
	Active material mass loading (mg cm^{-2}, each side)	26.48
	Electrode length (mm)	56
	Electrode width (mm)	43
	Al foil thickness (μm)	16
	Layers	3
Li Metal Anode	Cell Balance (N/P ratio)	1.09
	Electrode thickness (single side) (μm)	50
	Layers	4
Electrolyte	Electrolyte/capacity (g Ah^{-1})	1.98
	Weight (g)	2.75
Separator	Thickness(μm)	16
Packaging Foil	weight (g)	4.07
Cell	Capacity (Ah)	1
	Cell weight (g)	9.9
	Energy density (Wh Kg^{-1})	302

Supplementary Table 4. Comparison of the thermal stability of lithium metal batteries with different electrolytes.

Electrolyte	T1 (°C)	T2 (°C)	Ref.
LiFSI:TBP:PFPN (1:1.2:5 by mol.)	185	224	This work
1.2M LiPF6 EC/DMC 1.2M LiPF6 EC/DMC with 10 DEA	84 84	112 179	Hang Li et al., ACS Appl. Mater. Interfaces, 2021, 13, 57142
1.2M LiFSI-BMC with 0.75 wt% LiNO3 1 wt% LiDFBOP 1 M LiPF6 in EC: DMC: EMC = 1:1:1 wt.%	155 110	161 158	Jiawei Chen et al. Nat. Commun. 2024, 15, 3217
1M LiPF6 EC/DEC	41.9	111	Feng-Ni Jiang et al., J. Energy. Chem., 2022, 72, 158
1M LiPF6 EC/DEC	72.7	88.2	Xiang-Qun Xu et al., SusMat, 2022, 2, 435

REFERENCES

1. Liao, L. Han Z.; Feng, X. et al. Non-flammable long chain phosphate ester based electrolyte via competitive solventized structures for high-performance lithium metal batteries, *Journal of Energy Chemistry*, **2024**, *97*, 156-165, 2095-4956, doi: 10.1016/j.jechem.2024.05.025.
2. Liao, L. Shen, Y. Yang, Q. et al. Tailoring and unveiling the stable solvent structure dependence of interfacial chemistry for extremely high-temperature lithium metal batteries, *Journal of Energy Chemistry*, **2025**, *108*, 655-664, 2095-4956, doi: 10.1016/j.jechem.2025.04.055.
3. Li, M. et al. Multifunctional diluent regulated flame-retardant localized high concentration electrolyte boosting Li||NCM811 batteries, *Chemical Engineering Journal*, **2025**, *504*, 158923, 1385-8947, doi: 10.1016/j.cej.2024.158923.
4. Xiao, C. Wen, P. Luo, F. et al. Ultrahigh-Voltage Lithium Metal Batteries Enabled by Single-Ion and Weakly-Solvating Nanometric Aggregates. *Angew. Chem. Int. Ed.* **2025**, *64*, e202502465. doi: 10.1002/anie.202502465.
5. Song, J. Luo, P. Yang, Q. et al. Double-Weak Coordination Electrolyte Enables 5V and High Temperature Lithium Metal Batteries. *Small* **2025**, *21*, 2502620. doi: 10.1002/smll.202502620